ACS APPLIED MATERIALS & INTERFACES

Research Article

www.acsami.org

Grain-to-Grain Compositional Variations and Phase Segregation in Copper−Zinc−Tin−Sulfide Films

Alejandro Alvarez Barragan,[†] Hoda Malekpour,[‡] Stephen Exarhos,[†] Alexander A. Balandin,[‡,§] and Lorenzo Mangolini*[,†,‡]

[†]Department of Mechanical Engineering, [‡]Materials Science and Engineering Program, and [§]Department of Electrical and Computer Engineering, University of California−Riverside, Riverside, California 92521, United States

Supporting Information

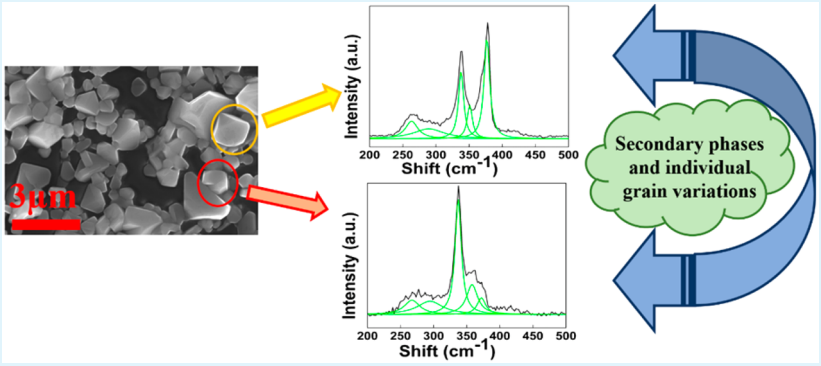

ABSTRACT: We have performed a rigorous investigation of the structure and composition of individual grains in copper−zinc−tin−sulfide (CZTS) films realized by sulfurization of a sputtered metal stack. Although on average close to the ideal CZTS stoichiometry, elemental analysis shows significant grain-to-grain variations in composition. High-resolution Raman spectroscopy indicates that this is accompanied by grain-to-grain structural variations as well. The intensity from the 337 cm^{-1} Raman peak, generally assigned to the kesterite phase of CZTS, remains constant over a large area of the sample. On the other hand, signals from secondary phases at 376 cm^{-1} (copper−tin−sulfide) and 351 cm^{-1} (zinc−sulfide) show significant variation over the same area. These results confirm the great complexity inherent to this material system. Moreover, structural and compositional variations are recognized in the literature as a factor limiting the efficiency of CZTS photovoltaic devices. This study demonstrates how a seemingly homogeneous CZTS thin film can actually have considerable structural and compositional variations at the microscale, and highlights the need for routine microscale characterization in this material system.

KEYWORDS: *CZTS, Raman spectroscopy, energy dispersive spectroscopy, phase segregation, thin films, earth-abundant photovoltaic materials*

INTRODUCTION

The number of studies on the quaternary chalcogenide Cu_2ZnSnS_4 has dramatically increased in the past decade. Its interesting electronic properties and the fact that is solely composed of earth-abundant elements have increased its popularity as a candidate for thin-film photovoltaic applications. The efficiency of various devices has already been reported.[1−5] Champion copper−zinc−tin−sulfide (CZTS)/CZTSSe cells have achieved efficiencies of 7.6% and 12.6% for sputtered metallic stacks and solution-based devices, respectively.[1,6] Although remarkable improvements have been made, these efficiency values are considerably lower than the theoretical limit of an ∼1.4 eV band gap material, which is close to 30%.[7] Among the main problems observed so far, low open-circuit voltage V_{OC} and low quantum efficiency are the most recurrent. The highest V_{OC} values reported for CZTS thin films fluctuate around 600 mV,[6,8,9] whereas its sister technology $Cu(In,Ga)Se_2$ has achieved up to 750 mV.[10,11] Moreover, quantum efficiency curves on CZTS devices have not reached 90% at optimal wavelengths and are usually accompanied by absorption and recombination losses in lower and higher energy regions.[1,8] Low V_{OC} on CZTS absorbers is usually attributed to deep recombination centers in the bulk material, interfaces, and grain boundaries,[12] while the presence of secondary phases with larger band gap contributes to a lower photocarrier generation.[9,13]

Energy-dispersive spectroscopy (EDS) and Raman scattering are two of the most utilized techniques for CZTS characterization. Most reports monitor the quality of their CZTS films by employing these techniques. Such measurements are usually conducted on larger areas of the sample rather than on individual grains. This procedure assumes that the film

Received: April 26, 2016
Accepted: August 18, 2016
Published: August 18, 2016

DOI: 10.1021/acsami.6b04982
ACS Appl. Mater. Interfaces 2016, 8, 22971−22976

stoichiometry and structure are the same for every grain present in it.[14,15] However, experimental results have shown that different Raman modes may be detected among CZTS microcrystals within the same sample.[16] Although this investigation focused on the sintering dynamics in films obtained from CZTS nanoparticle coatings, it suggests that structural inhomogeneity may be prevalent in this material system. In this manuscript, we present an in-depth EDS and Raman analysis of individual grains in order to shed light on inhomogeneities that have been so far overlooked.

EXPERIMENTAL SECTION

CZTS films were synthesized by sputtering a 250 nm film of Cu, Zn, and Sn stacked layers on a bare soda lime glass (SLG) substrate. The thickness of each layer was 80 nm (Cu), 60 nm (Zn), and 110 nm (Sn). The samples were then inserted in a quartz ampule together with a small charge (~1 mg) of elemental sulfur. The ampule was subsequently evacuated using a turbo pump and sealed at 10^{-5} Torr. The sample was heated up to 600 °C for 8 h and allowed to cool down naturally. This synthesis approach is very similar to those adopted by several other research groups.[4,17,18] Scanning electron microscopy (SEM)/EDS analysis was performed on a FEI Nova NanoSEM450 system equipped with Oxford Instruments Aztec Synergy software and a X-Max 50 mm^2 SDD detector with resolution of 127 nm at Mn Kα. For EDS characterization, the accelerating voltage was kept at 20 kV and the working distance at 5 mm. Raman characterization was conducted with two different instruments to compare individual-grain versus standard measurement results. A Renishaw micro-Raman spectrometer with a 488 nm excitation laser and a ~0.4 μm spot size was used for individual-grain characterization. A Horiba LabRam HR instrument equipped with a 532 nm laser source and an ~5 μm spot size was used to obtain the spectra of larger areas of the sample containing several grains. The spectra in both instruments were recorded with a 1800 lines/mm grating. The laser power was kept below 0.2 mW to avoid any local heating and damage to the sample. To improve the signal-to-noise ratio for such a small power, the exposure time was increased to 100 s. X-ray diffraction (XRD) characterization was held on a PANalytical Empyrean X-ray system using Cu Kα radiation with a wavelength of 1.54 Å.

RESULTS AND DISCUSSION

The elemental composition of the sample before sulfurization is presented in Table S1. SEM images of the film before and after annealing are shown in Figure S1 of the Supporting Information and Figure 1a,b, respectively. There is no clear trace of either ZnS or SnS_2 phases, which have been reported elsewhere as having very specific features that could be easily detectable with the aid of SEM microscopy.[19,20] The grain size ranges between 1 and 5 μm. This is not unexpected since impurities from the SLG substrate, more specifically, Na and K, have shown to enhance grain growth, most likely by diffusing into the grain boundaries and facilitating cation diffusion through several proposed mechanisms.[21−23] There is a substantial amount of voids along the sample. This is most likely due to a high material loss during the annealing process.[19] The Cu/Sn ratio before and after annealing went from 1 to ~1.8, indicating a large Sn loss. This phenomenon has been reported elsewhere.[19] EDS scans were performed over large areas of approximately 150 μm^2 that included several grains. The average composition and elemental ratios are displayed in Table 1. The recorded measurements show a stoichiometry very close to that of CZTS. In fact, there is a slightly Zn-rich composition that has proven beneficial for higher performance CZTS devices.[24−26] XRD and Raman characterization are shown in Figure 1c,d, respectively. The XRD data shows

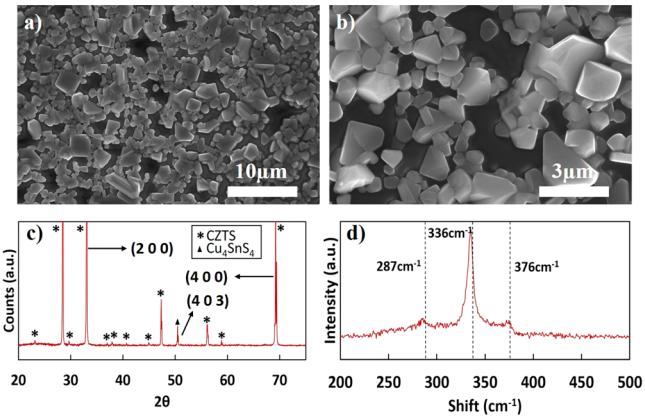

Figure 1. Standard characterization of seemingly phase-pure CZTS on a bare SLG substrate. (a), (b) SEM images at low and high magnification do not show obvious phase segregation of secondary phases such as ZnS or Sn_2S. (c) XRD reflections of the sample. Most reflections are in accordance with CZTS. Anomalous intensities detected at the (2 0 0) and (4 0 0) planes indicate preferential grain orientation on the film. The peak at 50.4° is definitely not CZTS, Cu_2SnS_3, nor ZnS and could be assigned to the Cu_4SnS_4 phase. (d) Representative Raman spectrum performed on a large area including several grains.

Table 1. Average Stoichiometry, Standard Deviation, and Elemental Ratios Obtained from EDS Characterization on Large Areas of the Sample

element	at. %	SD
Cu	24.67	±1.5
Zn	13.39	±0.6
Sn	14.14	±0.6
S	47.8	±1.2
Cu/(Zn + Sn)	Zn/Sn	S/metal
0.90	0.95	0.92

reflections at 28.5°, 32.9°, 47.2°, and 56.1°. These peaks are assignable to CZTS, but also to secondary phases such as Cu_2SnS_3 and ZnS. However, smaller peaks previously associated with only CZTS appear at 37.0° and 37.9°, suggesting that the analyzed film is mainly composed of CZTS. The peak at 50.4°, however, is unequivocally neither CZTS, Cu_2SnS_3, nor ZnS. The study in ref 18 provides a broad perspective on the major peaks from several binary and ternary sulfide phases that have been reported in the CZTS literature. Together with SnS_2, Cu_4SnS_4 is the only phase with a peak assigned at 50.4°. Raman analysis (Figure 1d) discards the presence of SnS_2 since its signature at 314 cm^{-1} is not present and could not be found in any of our scans. It is also worth noting anomalous intensities from the (2 0 0) and (4 0 0) CZTS planes. This is an indication of preferential grain orientation. For randomly oriented crystals, there is not known Cu−Sn−S (CTS) phase with only one main peak at 50.4°. The overlap between the CZTS peaks and those associated with secondary phases (Cu_2SnS_3 and ZnS) is an intensively discussed topic and calls for more conclusive CZTS characterization techniques.[27] A combination of Raman spectroscopy and EDS have been used as a more definitive approach for the identification of phase-pure CZTS. For this investigation, we applied a standard Raman spectra acquisition that uses a 532 nm laser with a ~5 μm spot size and compared it with a more thorough individual-grain characterization procedure explained

DOI: 10.1021/acsami.6b04982
ACS Appl. Mater. Interfaces 2016, 8, 22971−22976

below. For the standard method (large area), Raman spectra were obtained at random locations of the sample. There were no major differences between one another. Figure 1d is a representative measurement of all the spectra acquired under these conditions. There is a strong and narrow peak at 336 cm^{-1} and a weaker signal at 287 cm^{-1}. Both peaks correspond to the well-known CZTS Raman signature.[28,29] A weak shoulder is also visible at 376 cm^{-1} and may be associated with a CTS ternary phase. Cu_4SnS_4 has been previously assigned to this shift position.[18]

The analysis above is usually part of a standard set of characterization procedures used to identify CZTS films suitable for high-efficiency devices. From these results, it is tempting to conclude that the CZTS films have optimal composition and are phase-pure. A statistical analysis of the sample was carefully conducted by measuring the stoichiometry of individual CZTS grains by EDS. The scanned areas varied between 10 and 20 μm^2 depending on the grain size. Data was acquired from 20 individual grains picked at random. Figure 2

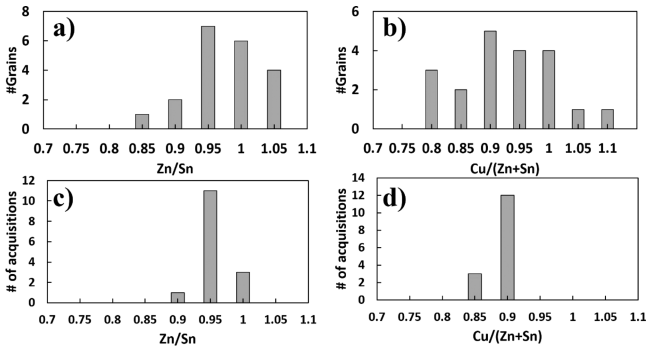

Figure 2. (a) Zn/Sn ratio and (b) Cu/(Zn + Sn) ratio distribution from an individual-grain EDS statistical analysis. (c) Zn/Sn ratio and (d) Cu/(Zn + Sn) ratio distribution from several acquisitions performed over the same grain.

shows the distribution of Zn/Sn and Cu/(Zn + Sn) ratios (Figure 2a,b, respectively) obtained from the 20 scans. There are significant changes in the grain-to-grain stoichiometry. The Zn/Sn ratio fluctuates between 1.04 and 0.84. The Cu/(Zn + Sn) ratio varies even more, ranging between 0.78 and 1.06, which indicates a more significant variation in copper concentration than in Zn and Sn. Raw values from this elemental analysis can be found in Table S2. Figure 2c,d displays the corresponding elemental ratio distribution from several acquisitions performed over the same grain. The resulting narrow spreads indicate that the EDS measurement reproducibility is sufficiently high to conclude that the variation in composition is not an instrument artifact. Moreover, we also found that the Cu stoichiometry appears to be closely related to that of sulfur. Figure 3 shows how the Cu/(Zn+Sn) ratio increases as the sulfur/metal ratio decreases. On the other hand, there does not seem to be any relation between the Zn/Sn ratio and the sulfur/metal ratio. A different visualization of this data is presented in Figure S2. EDS analysis may be influenced not only by grain composition but also by grain orientation when dealing with very anisotropic crystal structures. However, previous measurements on CZTS microfibers with different crystal orientations did not yield any significant variations on the EDS data.[30] In general, from EDS characterization we can conclude that there are evident changes

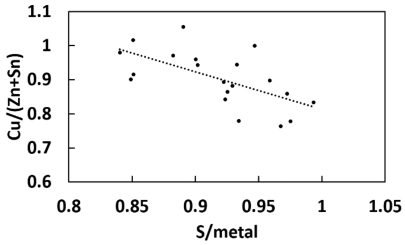

Figure 3. Scatter plot summarizing the correlation between copper and sulfur concentrations. Copper-rich regions tend to be sulfur-poor.

in grain-to-grain stoichiometry, proving that the seemingly homogeneous CZTS film assumption is not valid.

In similar fashion to the EDS analysis, additional Raman spectra were obtained for individual grains. A more precise Raman tool (details in Experimental Section) was used for capturing the Raman signature of grains large enough to be independently scanned. Figure 4 shows two representative

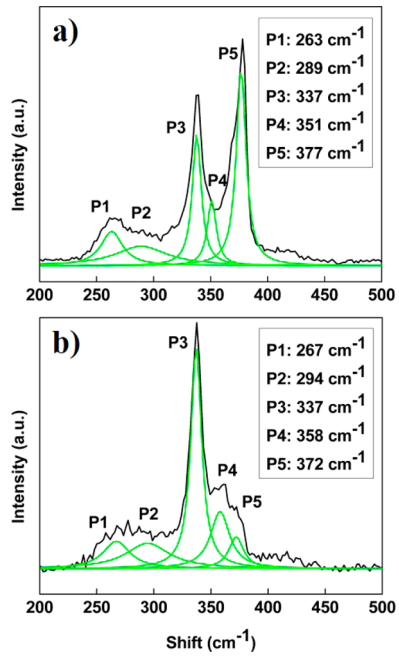

Figure 4. Representative Raman spectra from two distinct grains. A peak at (a) 376 cm^{-1} and a shoulder beginning at (b) 351 cm^{-1} appear sporadically, while the main CZTS peaks at 337 and 289 cm^{1} are present in every grain.

spectra from two different grains. In general, the 337 and 289 cm^{-1} intensity peaks are constant along various grains. However, peaks at 376 and 265 cm^{-1}, and a shoulder that extends from 351 to 362 cm^{-1}, are detected sporadically at every other grain. This finding suggests that major differences between individual CZTS grains are not detected with standard characterization procedures. The 376 cm^{-1} peak has previously been assigned to the Cu_4SnS_4 phase.[18] This strengthens the argument made for the XRD reflection at 50.4°, which does not correspond to neither CZTS, ZnS, nor Cu_2SnS_3. The shoulder at 351 cm^{-1} and the weak signal at 265 cm^{-1} can be associated with cubic ZnS.[28,31] In this case, XRD data cannot confirm this statement since the ZnS XRD signature overlaps with that of CZTS.

DOI: 10.1021/acsami.6b04982
ACS Appl. Mater. Interfaces 2016, 8, 22971−22976

Additional to the individual-grain study, the intensities of the peaks at 337, 351, and 376 cm^{-1} were analyzed with the high-resolution spectrometer by mapping an area of 200 μm^2. Figure 5b–d show maps that reveal the intensity variations of peaks at

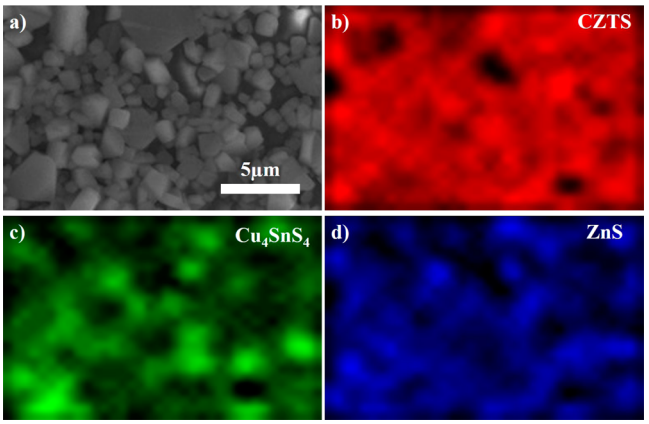

Figure 5. Intensity mapping of peaks at (b) 337 cm^{-1} (CZTS), (c) 376 cm^{-1} (Cu_4SnS_4), and (d) 351 cm^{-1} (ZnS). CZTS intensity peak remains relatively unchanged while the signal from the secondary phases fluctuates considerably. The scanned area in (a) is 200 μm^2.

337 (CZTS), 376 (Cu_4SnS_4), and 351 (ZnS) cm^{-1} over the scanned area. Except for the evident low signal coming from voids in the sample, the CZTS peak intensity remains steady. In contrast, there are notable intensity variations in the other two peaks, which account for signals from the secondary phases. Similar to EDS characterization, Raman intensity is also influenced by grain orientation. It could then be argued that these intensity variations are a result of scanning grains with different orientations rather than differences in composition. To refute this argument, Figure 6 shows the correlation between Raman spectra and EDS characterization obtained from two individual grains. The major ZnS Raman peak in Figure 6a is consistent with the excess Zn stoichiometry measured on this grain. On the other hand, there is no major hint of secondary phases in Figure 6b. Consequently, the resulting Zn/Cu ratio is close to that of stoichiometric CZTS, confirming that the acquired Raman data is dependent on grain stoichiometry and not on grain orientation. Data from Figure 5 and Figure 6, together with that of Figure 2 and Figure 4, strongly suggest that CZTS is the main phase in the system. However, there are still significant variations that involve the segregation of secondary phases that are likely to be detrimental in the performance of a CZTS device.

The results presented herein are consistent with theoretical predictions regarding the phase stability of CZTS and the influence of structural inhomogeneity on device performance. The narrow range of stability of CZTS and its tendency to segregate other binary and ternary phases are well-known issues.[12] Our findings suggest that such segregation is likely to occur at short-length scales so that careful microscopic characterization is needed to monitor the quality of CZTS films. With respect to device performance, previous theoretical studies attribute a low V_{OC} to compositional dissimilarities caused by point defects and the formation of secondary phases.[12,32,33] The fact that we unequivocally observe the presence of low band gap secondary phases like Cu_4SnS_4 (~1.2 ev[34]) is consistent with these studies. The presence of a wide band gap secondary phase such as ZnS (~3.7 ev[35]) is expected to reduce the light absorption of the film, decreasing photocurrent.[9,13]

CONCLUSIONS

We have performed an in-depth Raman and EDS analysis of individual CZTS grains. The results show a considerable variation in stoichiometry and Raman signal intensity that indicates the presence of secondary phases. Furthermore, the same sample also went through a standard characterization analysis that is commonly employed to report seemingly phase-pure homogeneous CZTS films. Contrary to the more rigorous individual-grain analysis, the results for the standard characterization did not yield evidence of compositional inhomogeneity. The contrasting data from both approaches suggests that the standard characterization procedures are not precise enough to detect grain-to-grain disparities. This issue should not be overlooked, given that the low-performance of CZTS-based devices is often attributed to compositional dissimilarities in the active layer. This work suggests that the routine use of microstructural characterization is necessary to advance this material system.

ASSOCIATED CONTENT

Supporting Information

The Supporting Information is available free of charge on the ACS Publications website at DOI: 10.1021/acsami.6b04982.

Stoichiometry of Zn/Cu/Sn precursor film before annealing, SEM image of Zn/Cu/Sn precursor film,

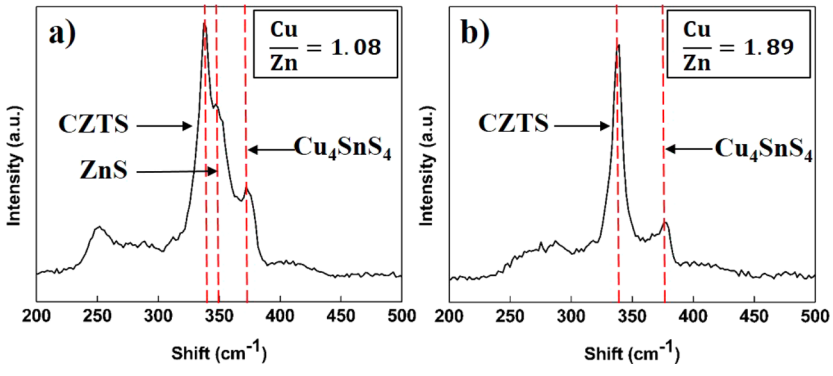

Figure 6. Correlation between Raman and EDS analysis. ZnS signal (350 cm^{-1}) in (a) is in good agreement with the Zn-rich stoichiometry measured for that grain. Low signal from secondary phases in (b) matches with a nearly stoichiometric CZTS grain.

DOI: 10.1021/acsami.6b04982
ACS Appl. Mater. Interfaces 2016, 8, 22971–22976

stoichiometry of several individual grains, and different visualization of copper−sulfur dependence (PDF)

AUTHOR INFORMATION

Corresponding Author

*E-mail: lmangolini@engr.ucr.edu.

Notes

The authors declare no competing financial interest.

ACKNOWLEDGMENTS

A. A. Barragan acknowledges the support of the "Consejo Nacional de Ciencia y Tecnología" (CONACYT, Mexico) and The University of California Institute for Mexico and the United States (UC MEXUS). S. Exarhos acknowledges the support of the National Science Foundation under award number 1545852 (PIRE). L. Mangolini acknowledges the support of the National Science Foundation under award number 1351386 (CAREER). A. A. Balandin acknowledges partial support from the National Science Foundation (NSF) via grants ECCS 1549942 and CMMI 1404967. Raman and XRD were performed at the Analytical Chemistry Instrumentation Facility (ACIF) at UC Riverside. SEM characterization was performed at the Central Facility for Advanced Microscopy and Microanalysis (CFAMM) at UC Riverside.

REFERENCES

(1) Wang, W.; Winkler, M. T.; Gunawan, O.; Gokmen, T.; Todorov, T. K.; Zhu, Y.; Mitzi, D. B. Device Characteristics of CZTSSe Thin-Film Solar Cells with 12.6% Efficiency. *Adv. Energy Mater.* **2014**, *4*, 1301465.

(2) Emrani, A.; Vasekar, P.; Westgate, C. R. Effects of Sulfurization Temperature on CZTS Thin Film Solar Cell Performances. *Sol. Energy* **2013**, *98*, 335−340.

(3) Mousel, M.; Schwarz, T.; Djemour, R.; Weiss, T. P.; Sendler, J.; Malaquias, J. C.; Redinger, A.; Cojocaru-Mirédin, O.; Choi, P.-P.; Siebentritt, S. Cu-Rich Precursors Improve Kesterite Solar Cells. *Adv. Energy Mater.* **2014**, *4*, 1300543.

(4) Dhakal, T. P.; Peng, C.; Tobias, R. R.; Dasharathy, R.; Westgate, C. R. Characterization of a CZTS Thin Film Solar Cell Grown by Sputtering Method. *Sol. Energy* **2014**, *100*, 23−30.

(5) Agawane, G. L.; Kamble, A. S.; Vanalakar, S. A.; Shin, S. W.; Gang, M. G.; Yun, J. H.; Gwak, J.; Moholkar, A. V.; Kim, J. H. Fabrication of 3.01% Power Conversion Efficient High-Quality CZTS Thin Film Solar Cells by a Green and Simple Sol−Gel Technique. *Mater. Lett.* **2015**, *158*, 58−61.

(6) Fukano, T.; Tajima, S.; Ito, T. Enhancement of Conversion Efficiency of Cu_2ZnSnS_4 Thin Film Solar Cells by Improvement of Sulfurization Conditions. *Appl. Phys. Express* **2013**, *6*, 062301.

(7) Shockley, W.; Queisser, H. J. Detailed Balance Limit of Efficiency of p-n Junction Solar Cells. *J. Appl. Phys.* **1961**, *32*, 510−519.

(8) Ahmed, S.; Reuter, K. B.; Gunawan, O.; Guo, L.; Romankiw, L. T.; Deligianni, H. A High Efficiency Electrodeposited Cu_2ZnSnS_4 Solar Cell. *Adv. Energy Mater.* **2012**, *2*, 253−259.

(9) Kumar, M.; Dubey, A.; Adhikari, N.; Venkatesan, S.; Qiao, Q. Strategic Review of Secondary Phases, Defects and Defect-Complexes in Kesterite CZTS−Se Solar Cells. *Energy Environ. Sci.* **2015**, *8*, 3134−3159.

(10) Jackson, P.; Hariskos, D.; Wuerz, R.; Kiowski, O.; Bauer, A.; Friedlmeier, T. M.; Powalla, M. Properties of $Cu(In,Ga)Se_2$ Solar Cells with New Record Efficiencies up to 21.7%. *Phys. Status Solidi RRL* **2015**, *9*, 28−31.

(11) Jackson, P.; Hariskos, D.; Lotter, E.; Paetel, S.; Wuerz, R.; Menner, R.; Wischmann, W.; Powalla, M. New World Record Efficiency for $Cu(In,Ga)Se_2$ Thin-Film Solar Cells Beyond 20%. *Prog. Photovoltaics* **2011**, *19*, 894−897.

(12) Polizzotti, A.; Repins, I. L.; Noufi, R.; Wei, S.-H.; Mitzi, D. B. The State and Future Prospects of Kesterite Photovoltaics. *Energy Environ. Sci.* **2013**, *6*, 3171−3182.

(13) Mendis, B. G.; Goodman, M. C. J.; Major, J. D.; Taylor, A. A.; Durose, K.; Halliday, D. P. The Role of Secondary Phase Precipitation on Grain Boundary Electrical Activity in Cu_2ZnSnS_4 (CZTS) Photovoltaic Absorber Layer Material. *J. Appl. Phys.* **2012**, *112*, 124508.

(14) Hlaing Oo, W. M.; Johnson, J. L.; Bhatia, A.; Lund, E. A.; Nowell, M. M.; Scarpulla, M. A. Grain Size and Texture of Cu_2ZnSnS_4 Thin Films Synthesized by Cosputtering Binary Sulfides and Annealing: Effects of Processing Conditions and Sodium. *J. Electron. Mater.* **2011**, *40*, 2214−2221.

(15) Ahmed, S.; Reuter, K. B.; Gunawan, O.; Guo, L.; Romankiw, L. T.; Deligianni, H. A High Efficiency Electrodeposited Cu_2ZnSnS_4 Solar Cell. *Adv. Energy Mater.* **2012**, *2*, 253−259.

(16) Chernomordik, B. D.; Béland, A. E.; Deng, D. D.; Francis, L. F.; Aydil, E. S. Microstructure Evolution and Crystal Growth in Cu_2ZnSnS_4 Thin Films Formed By Annealing Colloidal Nanocrystal Coatings. *Chem. Mater.* **2014**, *26*, 3191−3201.

(17) Hong, S.; Kim, C. Characteristics of Cu_2ZnSnS_4 Thin Films Fabricated by Sulfurization of Two Stacked Metallic Layers. *Mol. Cryst. Liq. Cryst.* **2014**, *602*, 134−143.

(18) Cheng, A.-J.; Manno, M.; Khare, A.; Leighton, C.; Campbell, S. A.; Aydil, E. S. Imaging and Phase Identification of Cu_2ZnSnS_4 Thin Films Using Confocal Raman Spectroscopy. *J. Vac. Sci. Technol., A* **2011**, *29*, 051203.

(19) Johnson, M. C.; Wrasman, C.; Zhang, X.; Manno, M.; Leighton, C.; Aydil, E. S. Self-Regulation of Cu/Sn Ratio in the Synthesis of Cu_2ZnSnS_4 Films. *Chem. Mater.* **2015**, *27*, 2507−2514.

(20) Alvarez, A.; Exarhos, S.; Mangolini, L. Tin Disulfide Segregation on CZTS Films Sulfurized at High Pressure. *Mater. Lett.* **2016**, *165*, 41−44.

(21) Nagaoka, A.; Miyake, H.; Taniyama, T.; Kakimoto, K.; Nose, Y.; Scarpulla, M. A.; Yoshino, K. Effects of Sodium on Electrical Properties in Cu_2ZnSnS_4 Single Crystal. *Appl. Phys. Lett.* **2014**, *104*, 152101.

(22) Prabhakar, T.; Jampana, N. Effect of sodium diffusion on the structural and Electrical Properties of Cu_2ZnSnS_4 Thin Films. *Sol. Energy Mater. Sol. Cells* **2011**, *95*, 1001−1004.

(23) Johnson, M.; Baryshev, S. V.; Thimsen, E.; Manno, M.; Zhang, X.; Veryovkin, I. V.; Leighton, C.; Aydil, E. S. Alkali-Metal-Enhanced Grain Growth in Cu_2ZnSnS_4 Thin Films. *Energy Environ. Sci.* **2014**, *7*, 1931−1938.

(24) Mitzi, D. B.; Gunawan, O.; Todorov, T. K.; Wang, K.; Guha, S. The Path Towards a High-Performance Solution-Processed Kesterite Solar Cell. *Sol. Energy Mater. Sol. Cells* **2011**, *95*, 1421−1436.

(25) Ki, W.; Hillhouse, H. W. Earth-Abundant Element Photovoltaics Directly from Soluble Precursors with High Yield Using a Non-Toxic Solvent. *Adv. Energy Mater.* **2011**, *1*, 732−735.

(26) Todorov, T. K.; Tang, J.; Bag, S.; Gunawan, O.; Gokmen, T.; Zhu, Y.; Mitzi, D. B. Beyond 11% Effi ciency: Characteristics of State-of-the-Art $Cu_2ZnSn(S,Se)_4$ Solar Cells. *Adv. Energy Mater.* **2013**, *3*, 34−38.

(27) Fernandes, P. A.; Salomé, P. M. P.; da Cunha, A. F. Study of polycrystalline Cu_2ZnSnS_4 films by Raman scattering. *J. Alloys Compd.* **2011**, *509*, 7600−7606.

(28) Fernandes, P. A.; Salomé, P. M. P.; Da Cunha, A. F. Growth and Raman Scattering Characterization of Cu_2ZnSnS_4 Thin Films. *Thin Solid Films* **2009**, *517*, 2519−2523.

(29) Himmrich, M.; Haeuseler, H. Far Infrared Studies on Stannite and Wurtzstannite Type Compounds. *Spectrochim. Acta Part A: Mol. Spectrosc.* **1991**, *47*, 933−942.

(30) Mu, C.; Song, Y.; Liu, A.; Wang, X.; Hu, J.; Ji, H.; Zhang, H. Electrospun Cu_2ZnSnS_4 Microfibers with Strong (112) Preferred Orientation: Fabrication and Characterization. *RSC Adv.* **2015**, *5*, 15749−15755.

(31) Nilsen, W. G. Raman Spectrum of Cubic Zns. *Phys. Rev.* **1969**, *182*, 838−850.

DOI: 10.1021/acsami.6b04982
ACS Appl. Mater. Interfaces 2016, 8, 22971−22976

(32) Chen, S.; Walsh, A.; Gong, X.-G.; Wei, S.-H. Classification of Lattice Defects in the Kesterite Cu_2ZnSnS_4 and $Cu_2ZnSnSe_4$ Earth-Abundant Solar Cell Absorbers. *Adv. Mater.* **2013**, *25*, 1522−1539.
(33) Niemegeers, A.; Burgelman, M.; De Vos, A. On the CdS/$CuInSe_2$ Conduction Band Discontinuity. *Appl. Phys. Lett.* **1995**, *67*, 843−845.
(34) Avellaneda, D.; Nair, M. T. S.; Nair, P. K. Cu_2SnS_3 and Cu_4SnS_4 Thin Films via Chemical Deposition for Photovoltaic Application. *J. Electrochem. Soc.* **2010**, *157*, D346−D352.
(35) Lippens, P. E.; Lannoo, M. Calculation of the Band Gap for Small CdS and ZnS Crystallites. *Phys. Rev. B: Condens. Matter Mater. Phys.* **1989**, *39*, 10935−10942.

DOI: 10.1021/acsami.6b04982
ACS Appl. Mater. Interfaces 2016, 8, 22971−22976